Electronic Supplementary Material

A tunable ionic covalent organic framework platform for efficient CO_2 catalytic conversion

Ting Li[1,2]*, Ji Xiong[1,2]*, Minghui Chen[1,2], Quan Shi[1,2], Xiangyu Li[1,2], Yu Jiang[1,2], Yaqing Feng[1,2], Bao Zhang **(✉)**[1,2,3]

1 School of Chemical Engineering and Technology, Tianjin University, Tianjin 300350, China

2 Guangdong Laboratory of Chemistry and Fine Chemical Industry Jieyang Center, Jieyang 522000, China

3 Haihe Laboratory of Sustainable Chemical Transformations, Tianjin 300192, China

*These authors contributed equally to this work.

E-mail: baozhang@tju.edu.cn

Content

Section 1. Experimental and characterization details

1.1 Reagents and materials

All chemicals and solvents, unless otherwise mentioned, are commercially available and used without further purification. All chemicals and reagents were used as received from commercial sources without further purification. Epichlorohydrin, epibromohydrin, butylene oxide, 1-allyloxy-2,3-epoxypropane, epoxy styrene, glycidyl phenyl ether, 1-butoxy-2,3-epoxypropane, mesitylene, N, N-dimethylformamide (DMF), N-butanol (*n*-BuOH), o-dichlorobenzene (o-DCB), Methanol, dimethylamine was purchased from Aladdin industrial corporation, Shanghai, China. Dichloromethane, acetone, hydrochloric acid, trifluoromethanesulfonic acid, 4-bromobenzonitrile, sodium hydroxide, saturated sodium bicarbonate, anhydrous sodium sulfate, 1,3,5-Trichloropyrimidine, 4-formylphenyl boronic acid, potassium carbonate and tetrakis(triphenylphosphine) palladium, petroleum ether, ethanol, 1,3,5-Tribromobenzene, 4-bromobenzaldehyde, 4-bromoacetophenone, ammonium acetate, acetic acid and *n*-BuLi, were purchased from Jiangtian chemical technology limited company, Tianjin, China.

1.2 Characterization techniques

Liquid ^{1}H Nuclear Magnetic Resonance (NMR) spectra of all monomers were recorded on a Bruker AVANCE IIITM HD 400 MHz NanoBAY. The solid ^{13}C NMR spectra were obtained on Japan Electronics JEOL JNM ECZ600R. Powder X ray diffraction (PXRD) data were collected on Netherlands the Panalytical X'Pert Pro using Cu Kα radiation at 40 kV, 40 mA power, the scanning angle is from 3-30 ° and the scanning speed is 0.1 °/s. Fourier-transform infrared (FTIR) spectra was measured on a

Nicolet 6700 instrument (400-3500 cm^{-1} region). Photoelectron spectrum data were measured on an X-ray photoelectron spectrometer of Thermo Fisher ESCALAB-250Xi. Thermogravimetric analysis (TGA) was measured on Netzsch TG 209F3 with heat rate of 10 ℃ in nitrogen atmosphere and the temperature measurement range is 30-800 ℃. The Brunauer-Emmett-Teller (BET) surface areas was measured by nitrogen adsorption and desorption at 77 K using Autosorb-iQ2-MP and the samples were activated at 120 ℃ for 12 h under vacuum before analysis, the degassing temperature is 120 ℃ and the degassing time is 6 h. The CHN elemental analysis was performed on an elemental analyzer Vario EL cube. The Br elemental analysis was performed on an inductively coupled plasma mass spectrometry NexION 300X. Field Emission Scanning Electron Microscopy (SEM) and energy dispersive spectroscopy (EDS) were measured on Hitachi S-4800, in order to avoid the influence of the C element on the carbon film, the sample was sonicated in petroleum ether and dropped onto the aluminum foil paper for EDS scanning. Transmission electron microscope (TEM) was measured on Japan Electronics JEM-2100F and JEM-F200.

Section 2. Synthetic Procedures

Synthesis of N-ethyl-2,4,6-trimethylpyridinium bromide (ETMP-Br)

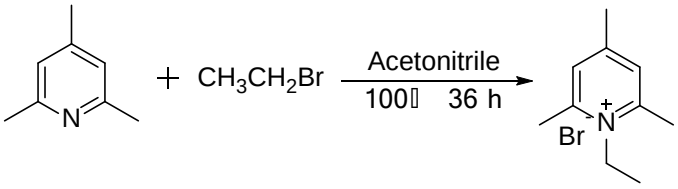

The synthetic route of ETMP-Br referred to the literature[1]. Bromoethane (6.02 mL, 80.0 mmol) was added dropwise to a solution of 2,4,6-trimethylpyridine (5 mL, 40.0 mmol) in acetonitrile (50 mL) at room temperature, which was also protected from light.

After stirring at 100 ℃ for 36 h, the solvent was evaporated to give a white solid, which was recrystallized in ethyl acetate to give 1.95 g product as white crystal with yield of 21.7 %. ^{1}H-NMR (400 MHz, $CDCl_3$) 7.60 (s, 2H), 4.78 (q, 2H, *J* = 7.4 Hz), 2.98 (s, 6H), 2.56 (s, 3H), 1.55 (t, 3H, *J* = 7.4 Hz).

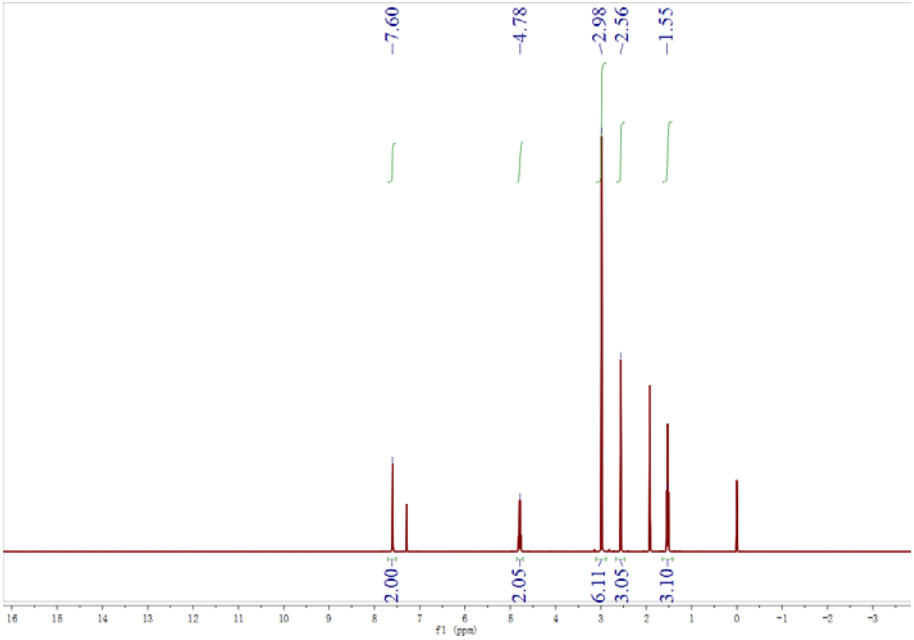

Fig. S1. The ^{1}H NMR spectrum of ETMP-Br.

Synthesis of 1,3,5-Tris(4-formylphenyl) triazine (TFPT)

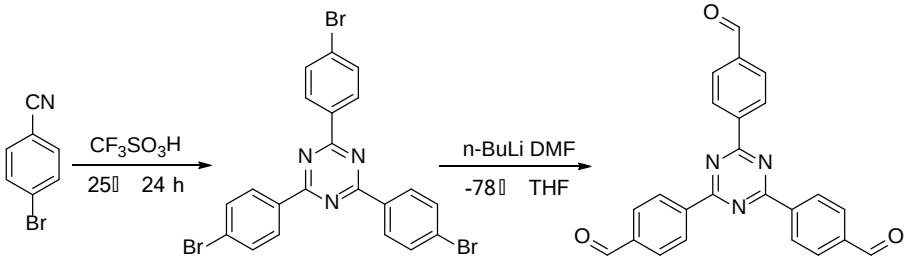

The synthetic route of TFPT referred to the literature[2]. In a 100 mL two neck-bottle , 3.5 mL (6 g, 40 mmol) trifluoromethanesulfonic acid was slowly added to 4-bromobenzonitrile (4 g, 22 mmol) at 0 ℃ and stirred for 30 min. After stirring at room temperature overnight, the resulting mixture was washed by 100 mL of deionized water and was neutralized by 5% NaOH water solution. After that, the precipitate was

collected by filtration and dried under vacuum oven at 100 ℃ for 12 h to yield 2,4,6-Tris(4-bromophenyl)-1,3,5-triazine as a white solid (3.96 g, 99.8%).

2,4,6-Tris(4-bromophenyl)-1,3,5-triazine (2.5 g, 4.58 mmol) was dissolved in dry tetrahydrofuran (250 mL) under a N_2 atmosphere. *n*-BuLi (2.5 M in n-hexane, 12 mL, 30.6 mmol) was added dropwise in the stirred solution at -78 ℃. After stirring for 3 h, N, N-dimethylformamide (9 mL) was added to the obtained black solution at -78 ℃ and the reaction mixture was further stirred for 12 h at room temperature. The resulting mixture was acidified with 3 M HCl aqueous solution (50 mL). The product was extracted with chloroform (150 mL), dried with anhydrous sodium sulphate and then evaporated under vacuum. The obtained mixture was recrystallized in the mixed petroleum ether and dichloromethane to afford 1,3,5-Tris(4-formylphenyl) triazine as white solid (0.78 g, 43.3%). ^{1}H NMR (400 MHz, $CDCl_3$) 10.20 (s, 3H), 8.98 (d, 6H, J = 8.3 Hz), 8.14 (d, 6H, J = 6.7 Hz).

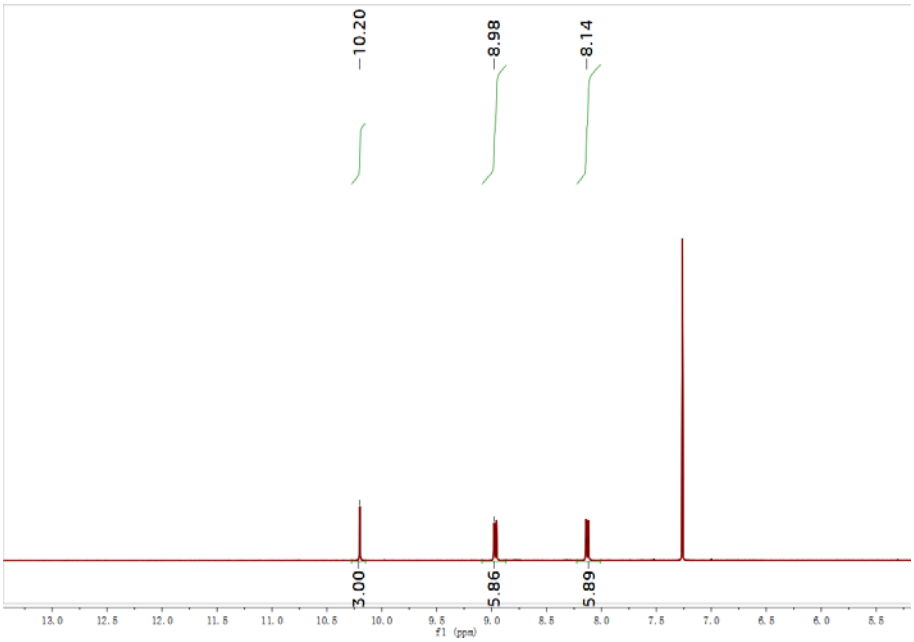

Fig. S2. The ^{1}H NMR spectrum of TFPT.

Synthesis of 1,3,5-Tris(4-formylphenyl) pyrimidine (TFPM)

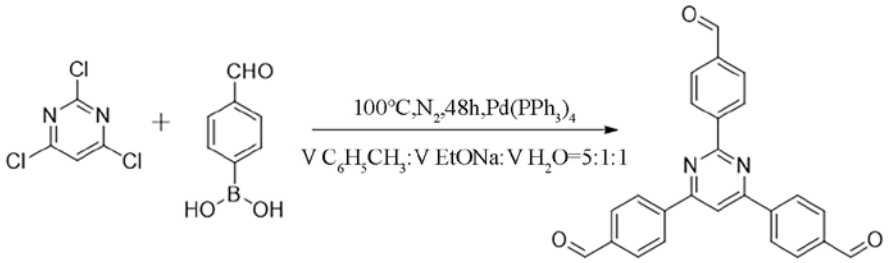

The synthetic route of TFPM referred to the literature. 1,3,5-Trichloropyrimidine (0.5 g, 2.73 mmol), 4-formylphenyl boronic acid (4.4 g, 29.3 mmol), potassium carbonate (4.2 g, 30.4 mmol) and tetrakis(triphenylphosphine) palladium (0.34 g, 0.30 mmol) were added to a 300 mL round bottom flask. The flask was evacuated and back filled with N_2 many times. Then the mixture solution of the toluene (100 mL), H_2O (20 mL) and ethanol (20 mL) were added to the flask. The reaction system was then heated to 100 ℃ and refluxed for 48 h. After cooling to room temperature, the precipitate was extracted with dichloromethane (200 mL) and dried with anhydrous sodium sulphate. Then the solvent was evaporated under vacuum. The product was purified by column chromatography using dichloromethane as the fluent phase. The resulting white solid was collected and dried in the vacuum oven at 80 ℃ for 12 h (0.32 g, 29.9%). ^{1}H NMR (400 MHz, $CDCl_3$) 10.17 (s, 3H), 8.90 (d, 2H, J = 6.7 Hz), 8.48 (d, 4H, J = 8.3 Hz), 8.20 (s, 1H), 8.13 (d, 6H, J = 8.4 Hz).

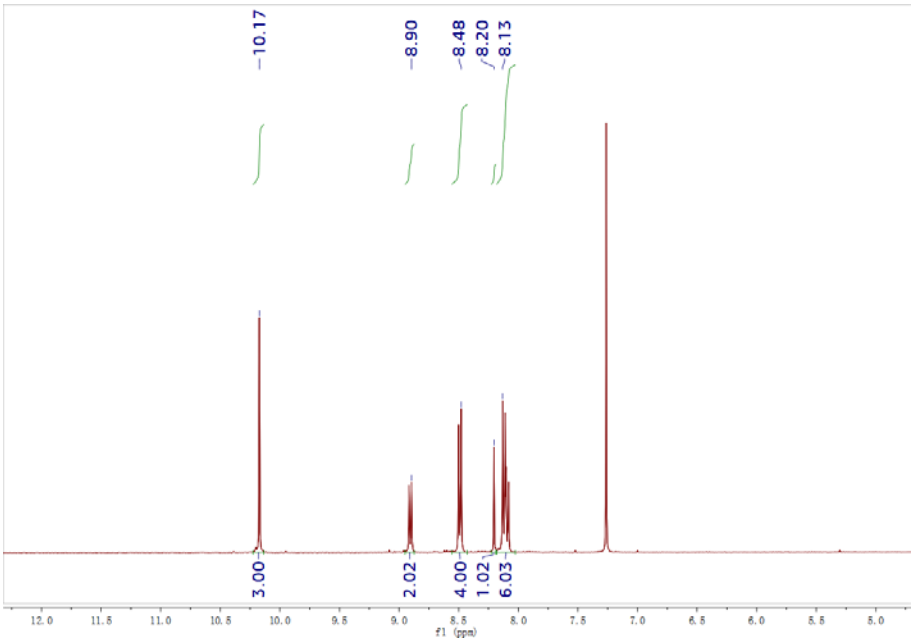

Fig. S3. The ^{1}H NMR spectrum of TFPM.

Synthesis of 1,3,5-Tris(4-formylphenyl) pyridine (TFPP)

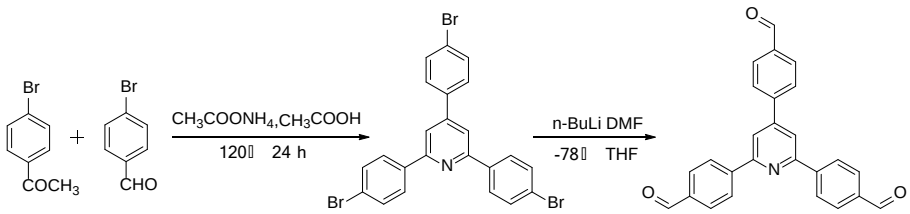

The synthetic route of TFPP referred to the literature[3]. A mixture of 4-bromobenzaldehyde (1.94 g, 10.5 mmol), 4-bromoacetophenone (4.14 g, 20.8 mmol), ammonium acetate (28 g, 363.2 mmol) and acetic acid (14.6 mL, 0.26 mmol) were added into a 300 mL round bottom flask. And then the reaction system was heated to 120 ℃ and refluxed for 24 h. After cooling to room temperature, deionized water (50 mL) was added, and the solution was neutralized by sodium bicarbonate ($NaHCO_3$) solution. 2,4,6-Tris(4-bromophenyl) pyridine was extracted with dichloromethane (150 mL), dried with anhydrous sodium sulphate and evaporated under vacuum. The product

was recrystallized with acetone and dried under vacuum overnight to yield a white solid of the product (1.23 g, 22.0%).

In a 250 mL two neck-bottle, 2,4,6-Tris(4-bromophenyl) pyridine (1 g, 1.84 mmol) was dissolved in dry tetrahydrofuran (250 mL) under a N_2 atmosphere. *n*-BuLi (2.5 M in n-hexane, 6 mL, 15.3 mmol) was added dropwise in the stirred solution at -78 ℃. After stirring for 3 h, N,N-dimethylformamide (4.5 mL) was added to the obtained black solution at -78 °C and the reaction mixture was further stirred for 12 h at room temperature. The resulting mixture was acidified with 3 M HCl aqueous solution (25 mL). The product was extracted with dichloromethane (150 mL), dried with anhydrous sodium sulphate, and then evaporated under vacuum. The product was purified with acetone to yield a white solid (0.3 g, 41.7%). ^{1}H NMR (400 MHz, $CDCl_3$) 10.14 (s, 3H), 8.39 (d, 4H, *J* = 7.6 Hz), 8.08 (d, 8H, *J* = 9.0 Hz), 7.95 (d, 2H, *J* = 7.7 Hz).

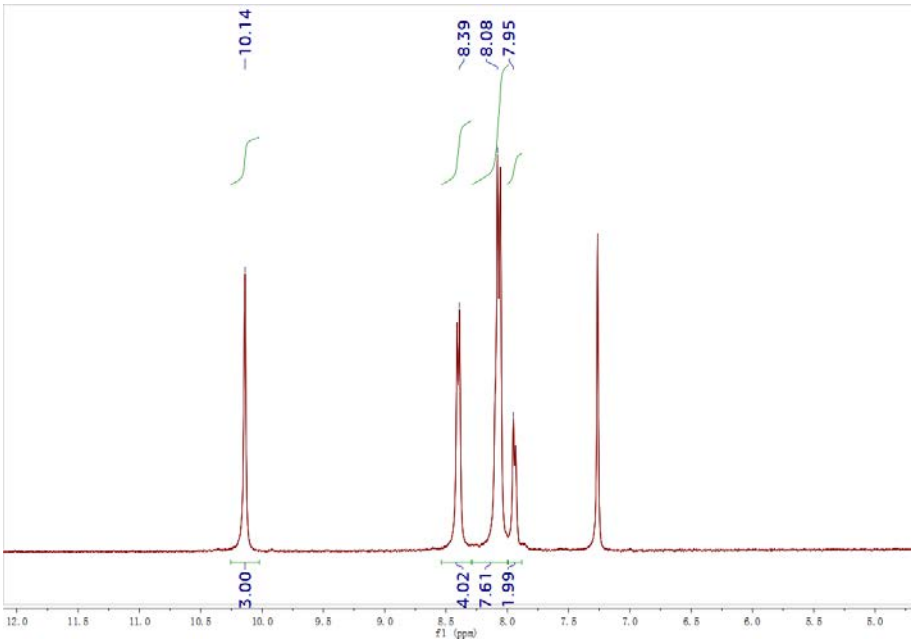

Fig. S4. The ^{1}H NMR spectrum of TFPP.

Synthesis of 1,3,5-Tris(4-formylphenyl) benzene (TFPB)

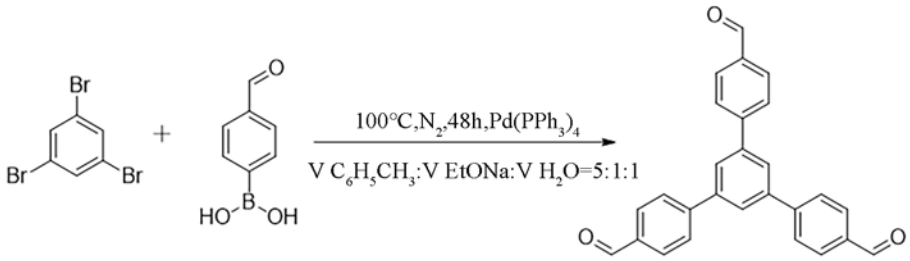

The synthetic route of TFPB referred to the literature[4]. 1,3,5-Tribromobenzene (5.0 g, 15.9 mmol), 4-formylphenyl boronic acid (14.3 g, 95.4 mmol), potassium carbonate (13.2 g, 95.5 mmol) and tetrakis(triphenylphosphine) palladium (0.92 g, 0.80 mmol) were added to a 300 mL round bottom flask. The flask was evacuated and back filled with N_2 many times. Then the mixture solution of the toluene (100 mL), H_2O (20 mL) and ethanol (20 mL) were added to the flask. The reaction system was then heated to 100 ℃ and refluxed for 48 h. After cooling to room temperature, the precipitate was extracted with dichloromethane (200 mL) and dried with anhydrous sodium sulphate. Then the solvent was evaporated under vacuum. The product was purified by column chromatography using dichloromethane as the fluent phase. The resulting white solid was collected and dried in in the vacuum oven at 80 ℃ for 12 h. (3.55 g, 57.2%). ^{1}H NMR (400 MHz, $CDCl_3$) 10.11 (s, 3H), 8.02 (d, 6H, J = 8.3 Hz), 7.92 (d, s, 3H), 7.88 (d, 6H, J = 8.3 Hz).

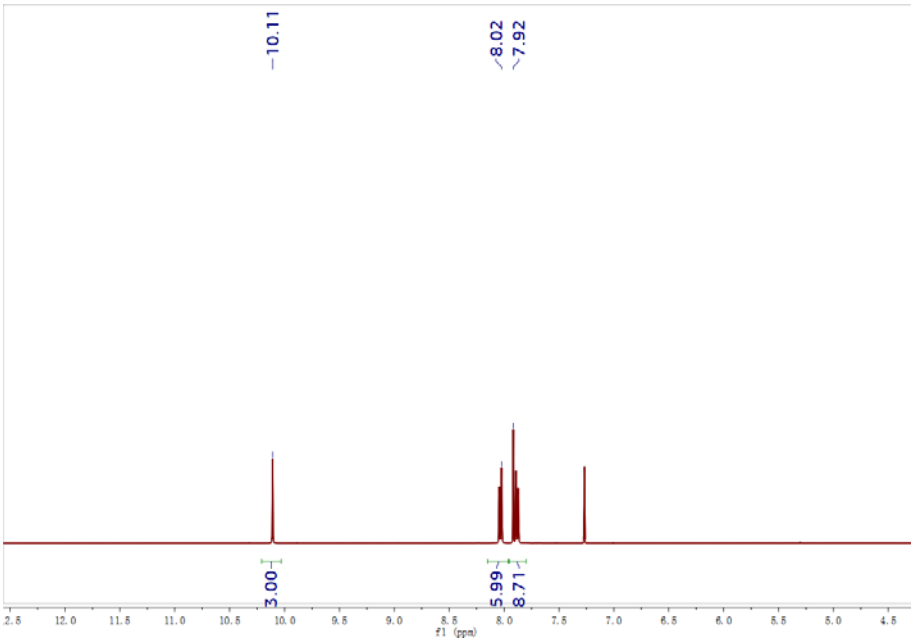

Fig. S5. The ^{1}H NMR spectrum of TFPB.

Synthesis of TME-COF

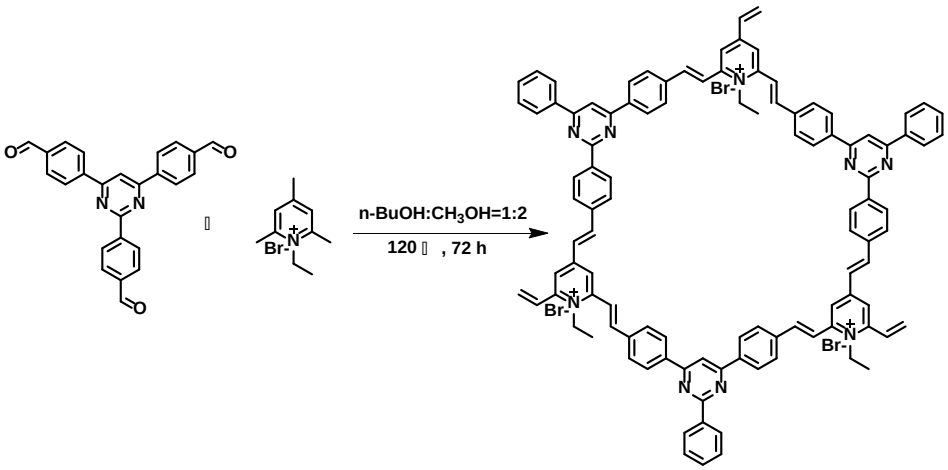

ETMP-Br (23.0 mg, 0.1 mmol) and TFPM (39.2 mg, 0.1 mmol) were dissolved in a mixture of 2.0 mL CH_3OH and 1.0 mL N-butanol (3 mL, v/v 2:1), and then bottled with a 10 mL Pyrex tube. And 2 M dimethylamine in anhydrous tetrahydrofuran solution (300 μL, 0.6 mmol) was added, followed by ultrasonication for 30 minutes. A yellow solution was resulted. The tube was placed into a Dewar filled with liquid N_2 and the solution was quickly frozen and degassed for 15 minutes. The tube was then dipped into

water to thaw the reaction system. The above operation was repeated three times to ensure that the air in the reaction system was completely removed. Then the glass tube was sealed with a flame and the yellow reaction solution was heated at 120 °C for 3 days. After cooling to room temperature, the yellow precipitate was collected by filtration and washed with the mixed solvent of 100 mL acetone and 100 mL tetrahydrofuran for three times, and then dried under vacuum at 60 ℃ for 12 h to obtain a yellow powder (yield: 76%).

Synthesis of TPE-COF

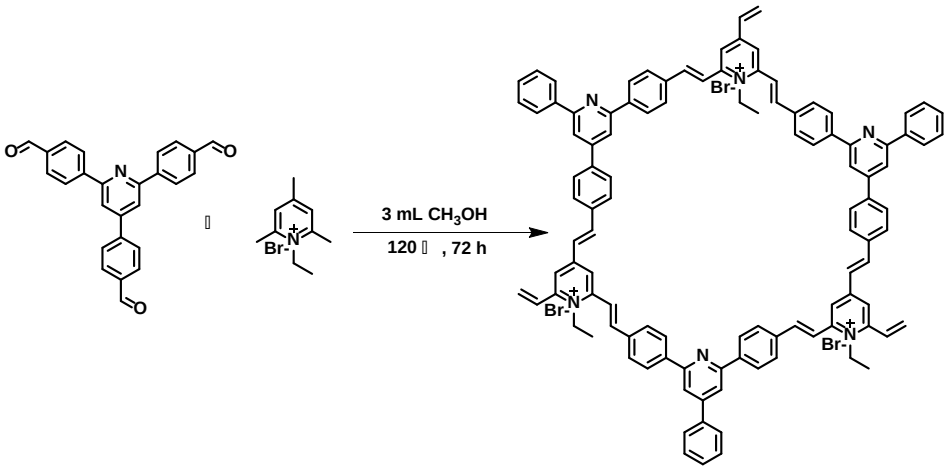

ETMP-Br (23.0 mg, 0.1 mmol) and TFPP (39.1 mg, 0.1 mmol) were dissolved in 3.0 mL CH_3OH, and then bottled with a 10 mL Pyrex tube. And 2 M dimethylamine in anhydrous tetrahydrofuran solution (300 μL, 0.6 mmol) was added, followed by ultrasonication for 30 minutes. A yellow solution was resulted. The tube was placed into a Dewar filled with liquid N_2 and the solution was quickly frozen and degassed for 15 minutes. The tube was then dipped into water to thaw the reaction system. The above operation was repeated three times to ensure that the air in the reaction system was completely removed. Then the glass tube was sealed with a flame and the yellow

reaction solution was heated at 120 °C for 3 days. After cooling to room temperature, the yellow precipitate was collected by filtration and washed with the mixed solvent of 100 mL acetone and 100 mL tetrahydrofuran for three times, and then dried under vacuum at 60 ℃ for 12 h to obtain a yellow powder (yield: 72%).

Synthesis of TBE-COF

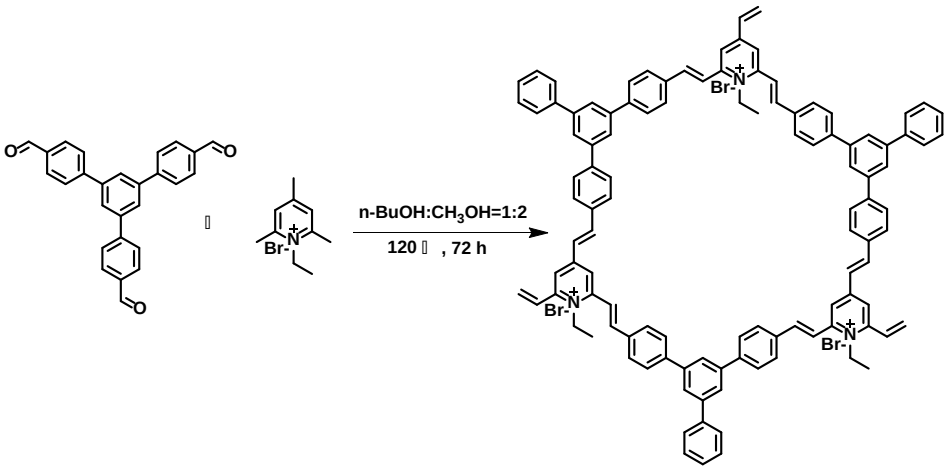

ETMP-Br (23.0 mg, 0.1 mmol) and TFPB (39.0 mg, 0.1 mmol) were dissolved in a mixture of 2.0 mL CH_3OH and 1.0 mL N-butanol (3 mL, v/v 2:1), and then bottled with a 10 mL Pyrex tube. And 2 M dimethylamine in anhydrous tetrahydrofuran solution (300 μL, 0.6 mmol) was added, followed by ultrasonication for 30 minutes. A yellow solution was resulted. The tube was placed into a Dewar filled with liquid N_2 and the solution was quickly frozen and degassed for 15 minutes. The tube was then dipped into water to thaw the reaction system. The above operation was repeated three times to ensure that the air in the reaction system was completely removed. Then the glass tube was sealed with a flame and the yellow reaction solution was heated at 120 °C for 3 days. After cooling to room temperature, the yellow precipitate was collected by filtration and washed with the mixed solvent of 100 mL acetone and 100 mL

tetrahydrofuran for three times, and then dried under vacuum at 60 ℃ for 12 h to obtain a yellow powder (yield: 80%).

Section 3. Exploration of synthesis conditions of COFs

Table S1. Exploring the synthesis conditions of TME-COF.

Control variable	Entry	Solvent systems /mL	Temprature /℃	Crystallinity
Solvent systems	1	DMF:o-DCB 2 M Dimethylamine=7:3:0.2	150	No
	2	DMF:*n*-BuOH 2 M Dimethylamine=1:1:0.2	150	No
	3	o-DCB:*n*-BuOH 2 M Dimethylamine=1:1:0.2	150	No
	4	*n*-BuOH:Mesitylene: 2 M Dimethylamine=1:1:0.2	150	No
	5	1,4-Dioxane:o-DCB: 2 M Dimethylamine=1:1:0.2	150	No
	6	1,4-Dioxane: *n*-BuOH: 2 M Dimethylamine=1:1:0.2	150	No
The amount of catalyst	7	*n*-BuOH:CH_3OH 2 M Dimethylamine=1:1:0.2	120	Moderate
	8	*n*-BuOH:CH_3OH 2M Dimethylamine=2:1:0.2	120	Low
	9	*n*-BuOH:CH_3OH 2 M Dimethylamine=1:2:0.2	120	Moderate
	10	*n*-BuOH:CH_3OH 2 M Dimethylamine=1:2:0.1	120	Moderate
	11	*n*-BuOH:CH_3OH 2 M Dimethylamine=1:2:0.3	120	High
Different catalyst	12	*n*-BuOH:CH_3OH 2 M NaOH=1:1:0.3	120	Unreacted
	13	*n*-BuOH:CH_3OH Cs_2CO_3=1:1:0.3	120	Unreacted

	14	*n*-BuOH:CH_3OH 2 M DBU=1:1:0.3	120	Unreacted

Table S2. Exploring the synthesis conditions of TPE-COF.

Control variable	Entry	Solvent systems /mL	Temprature /℃	Crystallinity
Solvent systems	1	DMF:o-DCB 2 M Dimethylamine=7:3:0.2	150	No
	2	DMF:*n*-BuOH 2 M Dimethylamine=1:1:0.2	150	No
	3	o-DCB:*n*-BuOH 2 M Dimethylamine=1:1:0.2	150	No
	4	*n*-BuOH:CH_3OH 2 M Dimethylamine=1:1:0.2	120	Low
	5	*n*-BuOH:CH_3OH 2 M Dimethylamine=2:1:0.2	120	Low
	6	*n*-BuOH:CH_3OH 2 M Dimethylamine=1:2:0.2	120	No
	7	*n*-BuOH:CH_3OH 2 M Dimethylamine=1:3:0.2	120	Moderate
	8	*n*-BuOH:CH_3OH 2 M Dimethylamine=1:5:0.2	120	Moderate
The amount of catalyst	9	CH_3OH 2 M Dimethylamine=10:1	120	High
	10	CH_3OH 2 M Dimethylamine=10:2	120	Moderate
	11	CH_3OH 2 M Dimethylamine=10:3	120	Low
Different catalyst	12	CH_3OH 2 M NaOH=10:1	120	Unreacted
	13	CH_3OH Cs_2CO_3=10:1	120	Unreacted
	14	CH_3OH 2 M DBU=10:1	120	Unreacted

Table S3. Exploring the synthesis conditions of TBE-COF.

Control variable	Entry	Solvent systems /mL	Temprature /℃	Crystallinity
Solvent systems	1	DMF:o-DCB 2 M Dimethylamine=7:3:0.2	150	No
	2	DMF:*n*-BuOH 2 M Dimethylamine=1:1:0.2	150	No
	3	o-DCB:*n*-BuOH 2 M Dimethylamine=1:1:0.2	150	No
	4	*n*-BuOH:Mesitylene: 2 M Dimethylamine=1:1:0.2	150	No
	5	1,4-Dioxane:o-DCB: 2 M Dimethylamine=1:1:0.2	150	No
	6	1,4-Dioxane: *n*-BuOH: 2 M Dimethylamine=1:1:0.2	150	No
The amount of catalyst	7	*n*-BuOH:CH_3OH 2 M Dimethylamine=1:1:0.2	120	Low
	8	*n*-BuOH:CH_3OH 2 M Dimethylamine=2:1:0.2	120	Low
	9	*n*-BuOH:CH_3OH 2 M Dimethylamine=1:2:0.2	120	Moderate
	10	*n*-BuOH:CH_3OH 2 M Dimethylamine=1:2:0.1	120	Moderate
	11	*n*-BuOH:CH_3OH 2 M Dimethylamine=1:2:0.3	120	High
Different catalyst	12	*n*-BuOH:CH_3OH 2 M NaOH=1:1:0.3	120	Unreacted
	13	*n*-BuOH:CH_3OH Cs_2CO_3=1:1:0.3	120	Unreacted
	14	*n*-BuOH:CH_3OH 2 M DBU=1:1:0.3	120	Unreacted

Section 4. Structural simulation

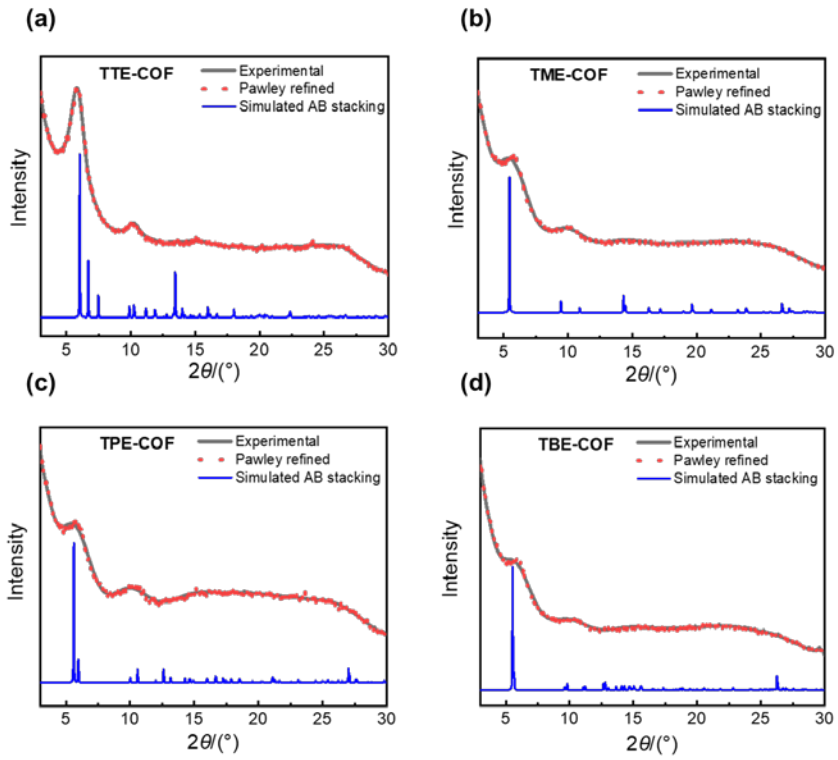

Fig. S6. Simulated AB stacking crystal structure of the TE-COFs.

Table S4. Atomic space position of the AA-stacking mode of TTE-COF and TME-COF.

AA-stacking mode Space group: P1 TTE-COF a=18.6454 Å, b=18.6443 Å, c=3.6180 Å α=90°, β=90°, γ=120°				AA-stacking mode Space group: P1 TME-COF a=18.6763 Å, b=18.6857 Å, c=3.6180 Å α=90°, β=90°, γ=120°			
	x	*y*	*z*		*x*	*y*	*z*
C1	0.64129	-1.77697	0.00235	C1	0.64142	-1.77655	4E-4
C2	0.69049	-1.81324	-0.05444	C2	0.69059	-1.81274	0.05674
N3	0.77515	-1.76418	-0.08156	N3	0.77503	-1.76383	0.08473
C4	0.81249	-1.67995	-0.02138	C4	0.81234	-1.67987	0.02338
C5	0.76391	-1.64304	0.02953	C5	0.76388	-1.64291	-0.02698
C6	0.67773	-1.69155	0.03563	C6	0.67779	-1.69125	-0.03211

C7	0.90329	-1.62381	-0.01039	C7	0.90301	-1.62432	0.01003
C8	0.651	-1.90421	-0.07795	C8	0.65154	-1.90345	0.0784
C9	0.62399	-1.65504	0.06291	C9	0.62404	-1.6548	-0.05869
C10	0.824	-1.79949	-0.23169	C10	0.82362	-1.79905	0.23729
C11	0.82733	-1.86239	0.02349	C11	0.82767	-1.86149	-0.01747
C12	0.65312	-1.57361	0.0687	C12	0.6529	-1.57354	-0.0639
C13	0.59858	-1.53775	0.08044	C13	0.59834	-1.53777	-0.07555
C14	0.63407	-1.45163	0.06994	C14	0.63372	-1.45181	-0.06602
C15	0.58384	-1.41565	0.0646	C15	0.58357	-1.41587	-0.06176
C16	0.49733	-1.46544	0.06947	C16	0.49718	-1.46549	-0.06672
C17	0.46187	-1.55178	0.08265	C17	0.46182	-1.55167	-0.07865
C18	0.51205	-1.58775	0.0876	C18	0.51194	-1.5876	-0.08256
C19	0.44416	-1.42773	0.05435	C19	0.44406	-1.42777	-0.0536
N20	0.47841	-1.34418	0.02677	N20	0.47843	-1.3441	-0.02845
C21	0.42946	-1.30944	0.00829	C21	0.43047	-1.30824	-0.01195
N22	0.34592	-1.3588	0.01716	C22	0.34482	-1.35812	-0.02042
C23	0.31098	-1.44222	0.04415	C23	0.30978	-1.44348	-0.0456
N24	0.36036	-1.47643	0.06268	N24	0.36016	-1.47657	-0.06173
C25	0.22023	-1.49492	0.04924	C25	0.21902	-1.49662	-0.05076
C26	0.4662	-1.21897	-0.01759	C26	0.46768	-1.21765	0.01225
C27	0.55213	-1.16731	-0.0449	C27	0.55347	-1.16619	0.0407
C28	0.58653	-1.08147	-0.06121	C28	0.58785	-1.08045	0.05744
C29	0.53534	-1.0462	-0.05068	C29	0.53675	-1.04519	0.04627
C30	0.44964	-1.09768	-0.02523	C30	0.45133	-1.09636	0.01925
C31	0.41529	-1.18352	-0.00965	C31	0.4171	-1.18185	0.00326
C32	0.16972	-1.4595	0.00874	C32	0.16818	-1.46158	-0.01177
C33	0.08361	-1.50923	0.00851	C33	0.08238	-1.51114	-0.01192
C34	0.04706	-1.59518	0.04967	C34	0.04606	-1.59679	-0.05208
C35	0.09722	-1.63065	0.09148	C35	0.09625	-1.63216	-0.09247
C36	0.18335	-1.58088	0.09109	C36	0.18233	-1.5824	-0.09167

C37	0.57	-1.95608	-0.04724	C37	0.57092	-1.95539	0.04434
C38	0.9571	-1.64994	0.04398	C38	0.95624	-1.65102	-0.04545
Br39	0.21626	-2.26873	-0.49952	Br39	0.21685	-2.26942	0.49381

Table S5. Atomic space position of the AA-stacking mode of TPE-COF and TBE-COF.

AA-stacking mode Space group: P1 TPE-COF a=18.5900 Å, b=18.8358 Å, c=3.6186 Å α=90°, β=90°, γ=120°				AA-stacking mode Space group: P1 TBE-COF a=18.7482 Å, b=18.7471 Å, c=3.6197 Å α=90 °, β=90°, γ=120°			
	x	*y*	*z*		*x*	*y*	*z*
C1	0.63941	-1.77806	0.002	C1	0.64177	-1.77668	0.00206
C2	0.68906	-1.8137	-0.05442	C2	0.69067	-1.81279	-0.05481
N3	0.77393	-1.76494	-0.08172	N3	0.77487	-1.76403	-0.08194
C4	0.81113	-1.68164	-0.02113	C4	0.81203	-1.68026	-0.02186
C5	0.7622	-1.64533	0.02958	C5	0.76375	-1.64352	0.02913
C6	0.67576	-1.69347	0.03512	C6	0.67805	-1.69173	0.03537
C7	0.90213	-1.62591	-0.0098	C7	0.90233	-1.62444	-0.01111
C8	0.65001	-1.90367	-0.0772	C8	0.65133	-1.90327	-0.07855
C9	0.62187	-1.65721	0.06165	C9	0.62464	-1.65539	0.06271
C10	0.82314	-1.79961	-0.2323	C10	0.82344	-1.79918	-0.23181
C11	0.82701	-1.86156	0.02299	C11	0.8267	-1.86173	0.02346
C12	0.65159	-1.57651	0.06852	C12	0.65365	-1.5744	0.06931
C13	0.59791	-1.53985	0.07946	C13	0.59944	-1.53871	0.08095
C14	0.63491	-1.45448	0.07255	C14	0.63477	-1.45308	0.07217
C15	0.58586	-1.41745	0.06698	C15	0.58485	-1.41727	0.06671
C16	0.49885	-1.46535	0.0679	C16	0.49866	-1.46661	0.0696
C17	0.46193	-1.55102	0.07742	C17	0.46356	-1.55258	0.08118
C18	0.51099	-1.58808	0.08264	C18	0.51341	-1.58838	0.08629
C19	0.44652	-1.42664	0.05313	C19	0.44561	-1.42883	0.05446

C20	0.48267	-1.34116	0.0275	C20	0.48038	-1.3431	0.02682
C21	0.43222	-1.30554	0.00955	C21	0.43053	-1.307	0.00798
C22	0.34615	-1.35664	0.01736	C22	0.34488	-1.35799	0.01677
C23	0.31124	-1.44155	0.04243	C23	0.30855	-1.44362	0.04377
N24	0.3621	-1.47419	0.05958	C24	0.35954	-1.47838	0.06246
C25	0.22014	-1.49498	0.04691	C25	0.21782	-1.49616	0.04879
C26	0.46826	-1.21565	-0.01455	C26	0.46717	-1.21657	-0.01755
C27	0.55431	-1.16338	-0.0454	C27	0.55267	-1.16499	-0.04852
C28	0.58768	-1.07854	-0.06126	C28	0.58695	-1.07962	-0.06457
C29	0.53545	-1.04466	-0.04691	C29	0.5362	-1.04444	-0.05031
C30	0.44976	-1.09646	-0.01786	C30	0.45104	-1.09553	-0.02143
C31	0.41646	-1.18124	-0.00269	C31	0.4168	-1.1809	-0.00603
C32	0.16812	-1.46128	0.00901	C32	0.16732	-1.46116	0.00625
C33	0.08199	-1.51152	0.00895	C33	0.08168	-1.51058	0.00623
C34	0.04659	-1.59646	0.04764	C34	0.0453	-1.59598	0.04964
C35	0.09802	-1.63042	0.08677	C35	0.09514	-1.63121	0.09353
C36	0.18435	-1.58003	0.08625	C36	0.18079	-1.58174	0.09298
C37	0.56903	-1.95564	-0.04356	C37	0.57079	-1.9548	-0.04643
C38	0.95649	-1.65141	0.04207	C38	0.95583	-1.65042	0.04423
Br39	0.21528	-2.2713	-0.49517	Br39	0.21763	-2.26944	-0.49794

Section 5. Geometry Optimization of Monomers

Table S6. DFT geometry optimizations of precursor aldehydes[5].

	Aldehyde	**Dihedral angle (deg):**		
		A	**B**	**C**
1	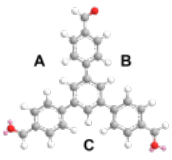	38.7	38.7	38.7

2	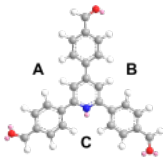	20.0	20.9	38.9
3	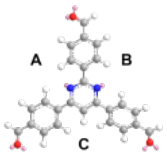	16.7	17.9	0.5
4	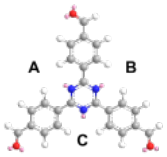	0	0	0

For the Knoevenagel condensation reaction, the reaction is irreversible. Therefore, the planarity of the building blocks is the main factor affecting the crystallinity of the prepared COFs. With the decrease of the number of nitrogen atoms of the central aromatic ring of triphenyl aryl platform, the dihedral angle between the central aromatic ring and the surrounding benzene ring changes (Table S6), resulting in the decrease of the planarity of the monomer. This will greatly affect the crystallinity of the prepared COFs.

Section 6. FTIR of TE-COFs

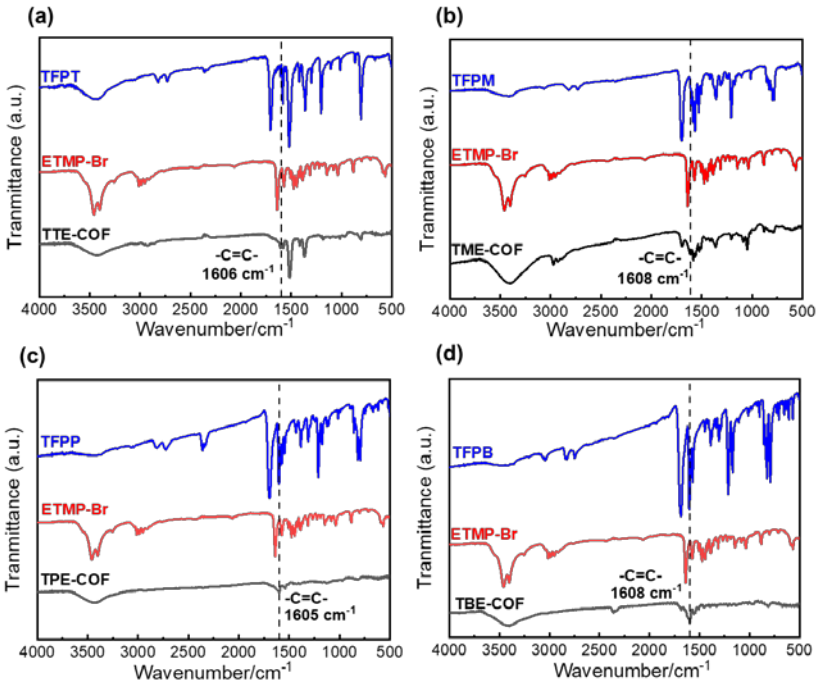

Fig. S7. The FT-IR spectra of TE-COFs.

Section 7. Zeta potential of TE-COFs

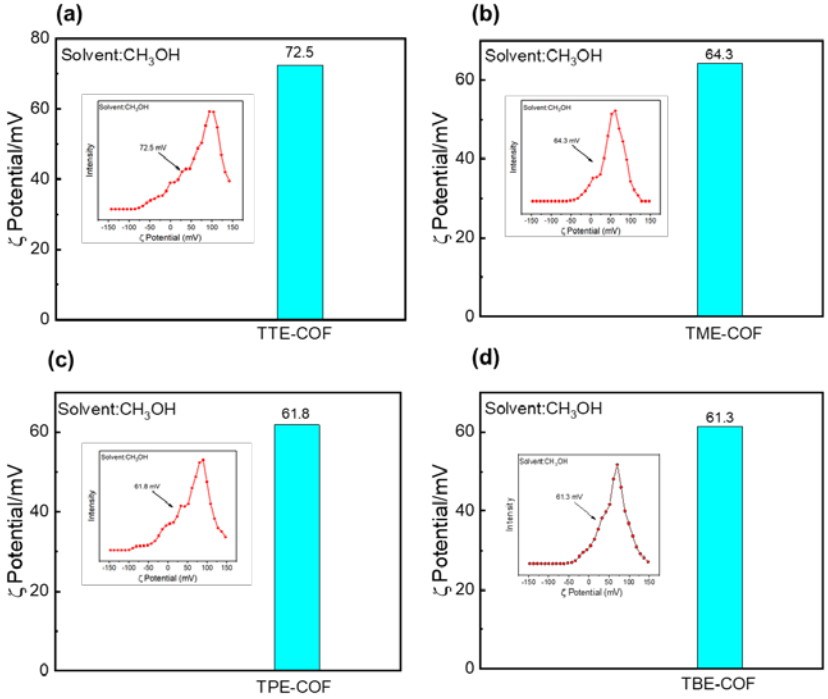

Fig. S8. Zeta potential of TE-COFs.

Section 8. The stability test of TE-COFs

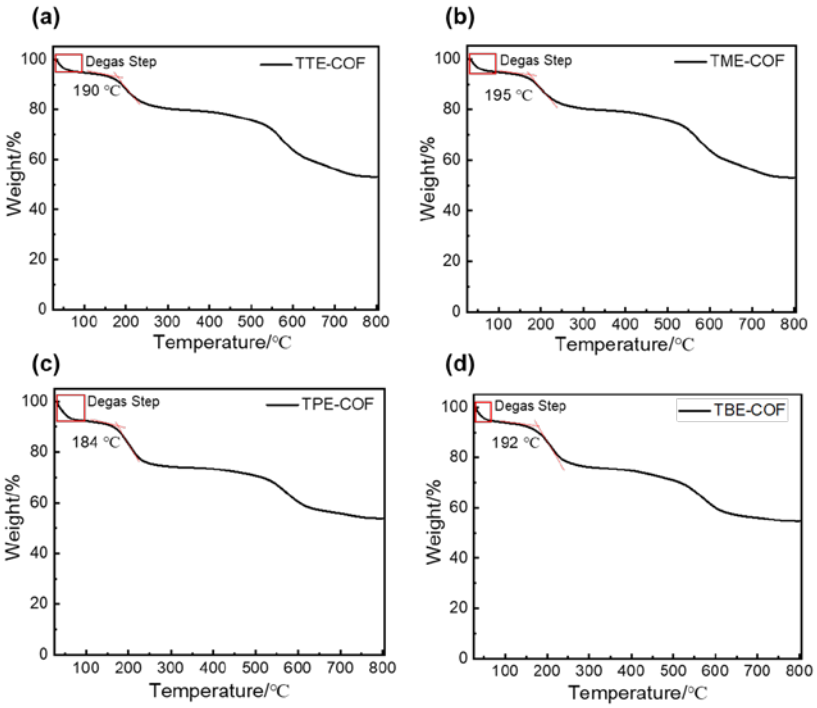

Fig. S9. The thermogravimetric analysis (TGA) curve of TE-COFs.

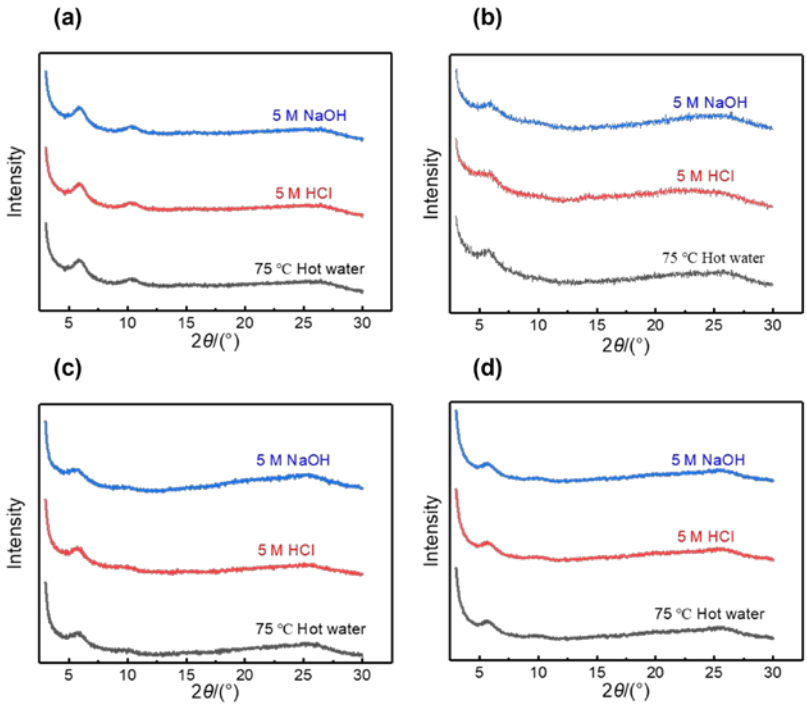

Fig. S10. Chemical stability test of TE-COFs.

Section 9. XPS of TE-COFs

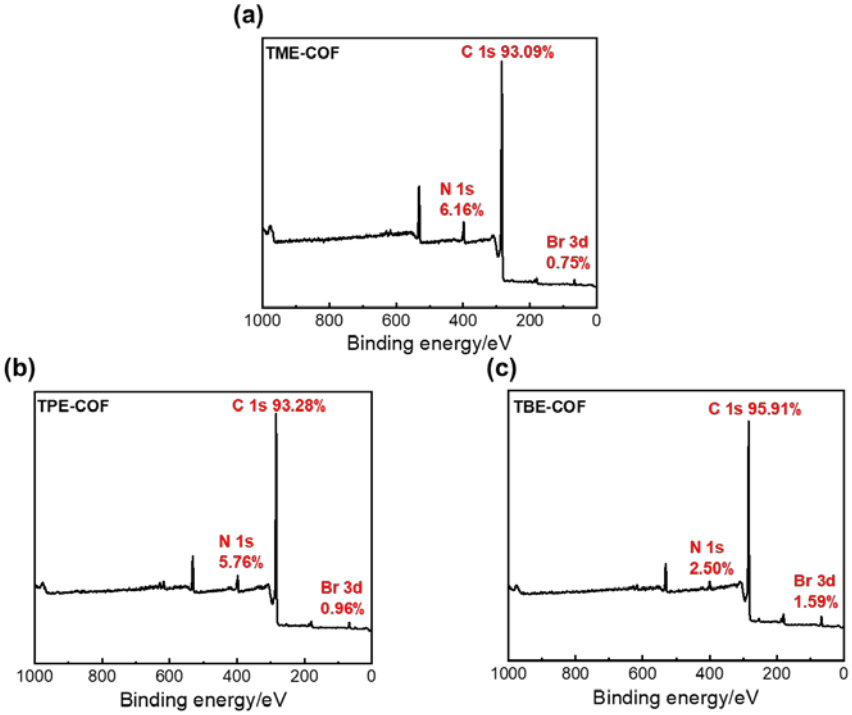

Fig. S11. XPS survey spectra of (a)TME-COF, (b) TPE-COF, (c) TBE-COF.

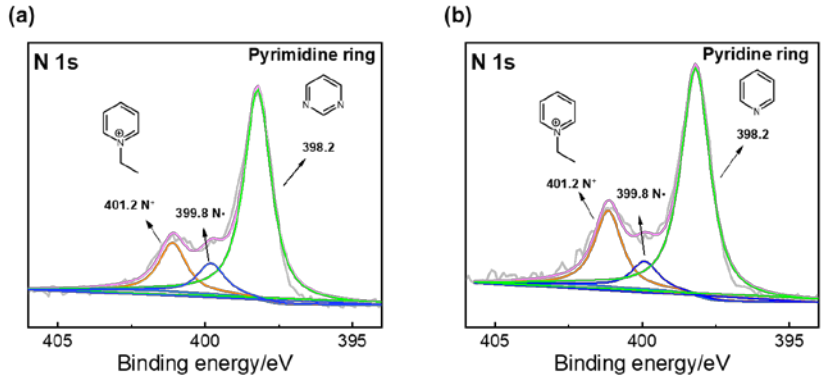

Fig. S12. High-resolution N 1s XPS spectra of (a) TME-COF, (b) TPE-COF.

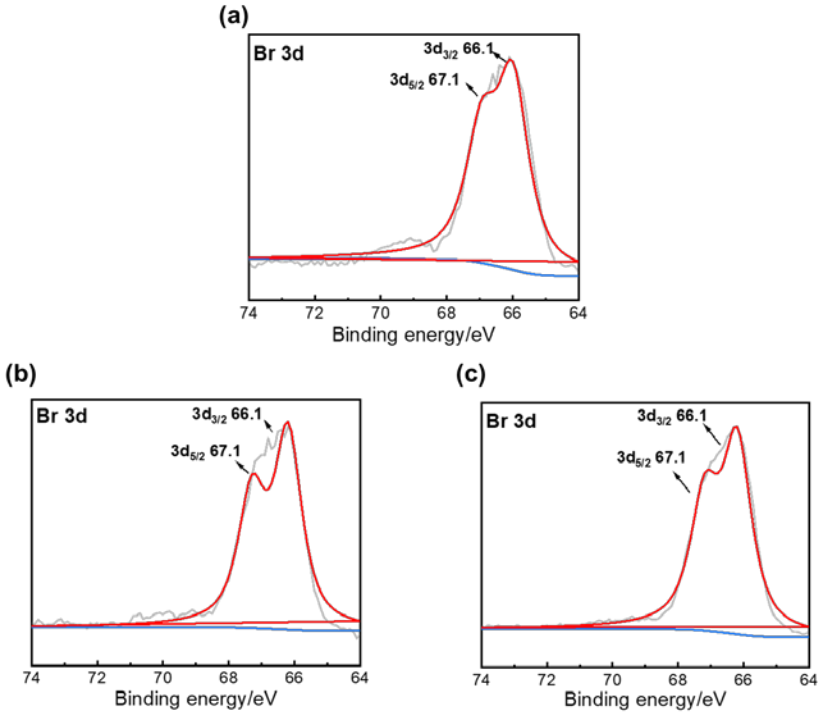

Fig. S13. High-resolution Br 3d XPS spectra of (a) TME-COF, (b) TPE-COF, (c) TBE-COF.

Section10. Elemental analysis of TE-COFs

Table S7. Elemental analysis of TE-COFs

Frameworks	Experimental (wt.%)				Theoretical (wt.%)			
	N	C	H	Br	N	C	H	Br
TTE-COF	9.03	72.10	5.07	11.64	9.84	71.71	4.42	14.03
TME-COF	6.51	74.98	5.56	11.12	7.39	73.94	4.61	14.05
TPE-COF	4.40	76.25	5.68	11.29	4.94	76.19	4.80	14.08
TBE-COF	2.33	77.85	5.76	12.15	2.45	78.44	4.98	14.10

Section 11. Summary of studies of CO_2 adsorption

Table S8. Comparison with the previous catalytic systems.

Entry	Catalyst	Temperature	CO_2 uptake(cm^3 g^{-1})	Ref.

1	COF1/$ZnBr_2$	273K	26.9	6
2	Zn/TPA-TCIF(BD)	273K	39.4	7
3	POM@ImTD-COF	273K	13	8
4	Al-iPOP-2	273K	33.4	9
5	AMIMBr@H2P-DHPhCOF	273K	31.9	10
6	$Phen^{\bullet+}$-PHP-2Br	273K	19.8	11
7	Py-iPOP-1	273K	18.2	12
8	CTF-0-400-40-1	273K	37.4	13
9	TTE-COF	273K	45.6	this work

Section 12. The isosteric heat (Q_{st}) plots of CO_2 adsorption

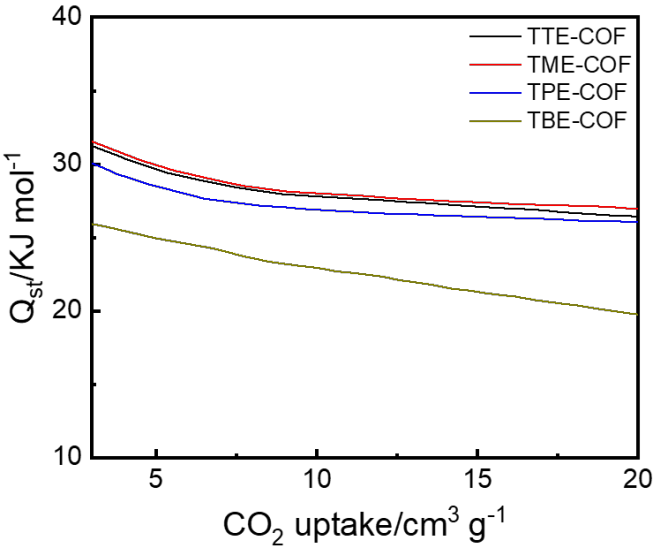

Fig. S14. The isosteric heat (Q_{st}) plots of CO_2 adsorption for TE-COFs calculated using the Clausius-Clapeyron equation.

Section 13. TEM images of TE-COFs

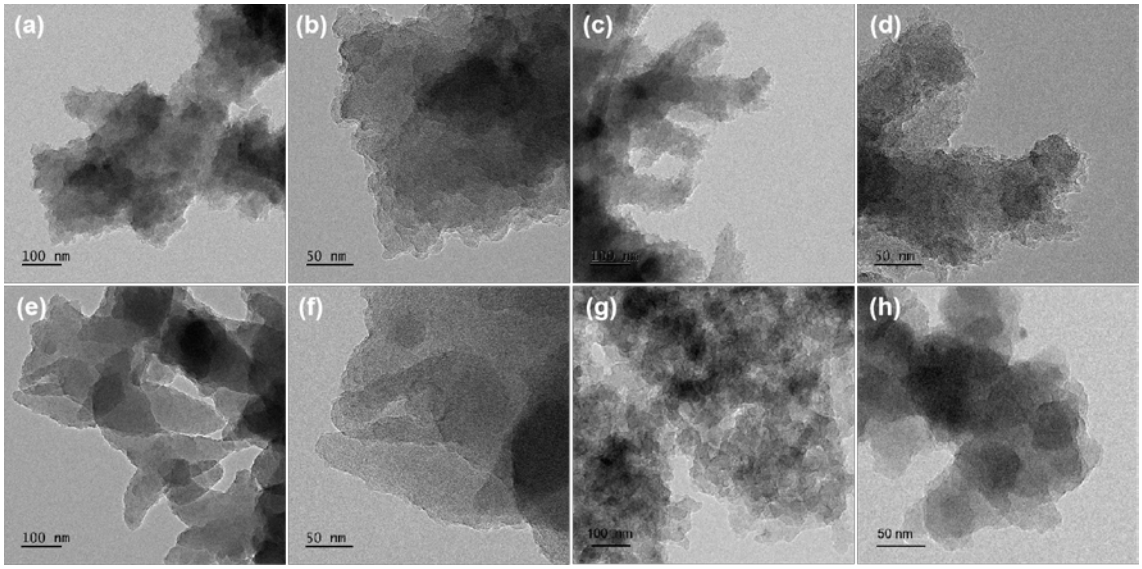

Fig. S15. TEM images of (a, b) TTE-COF, (c, d) TME-COF, (e, f) TPE-COF, (g, h) TBE-COF.

Section 14. EDS of TE-COFs

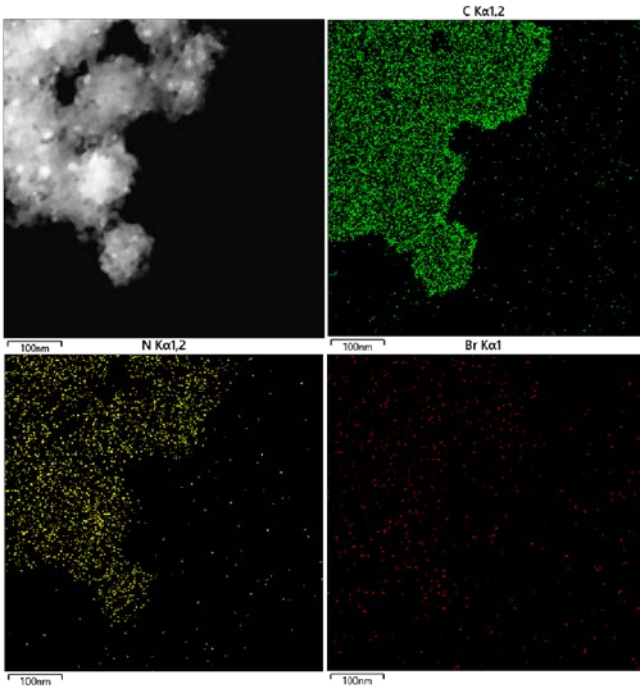

Fig. S16. EDS images of TTE-COF. Green, yellow and red respectively represent the three elements of C, N, Br.

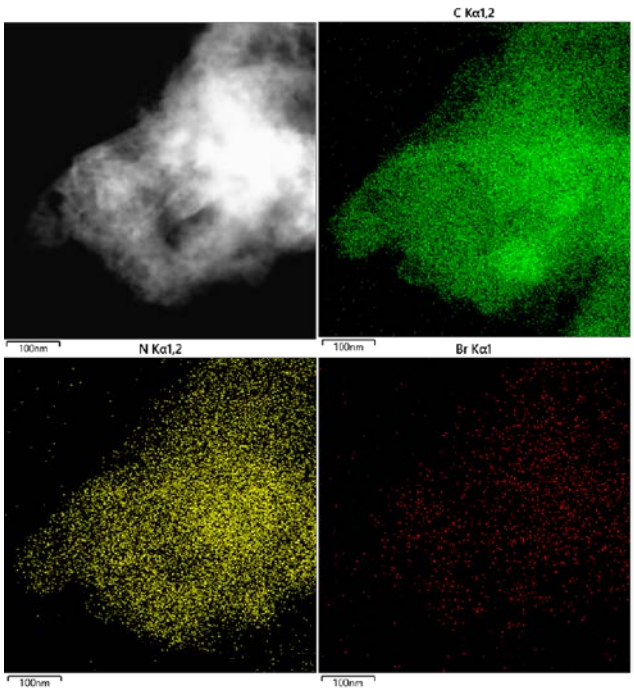

Fig. S17. EDS images of TME-COF. Green, yellow and red respectively represent the three elements of C, N, Br.

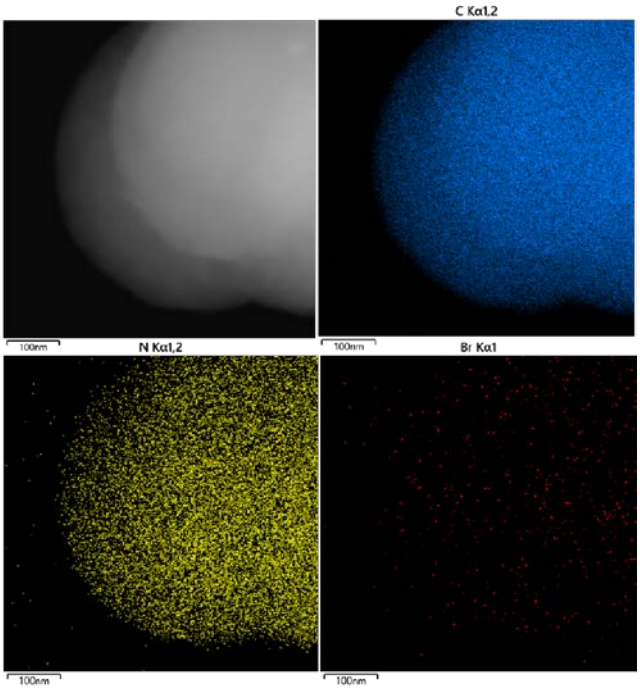

Fig. S18. EDS images of TPE-COF. Blue, yellow and red respectively represent the three elements of C, N, Br.

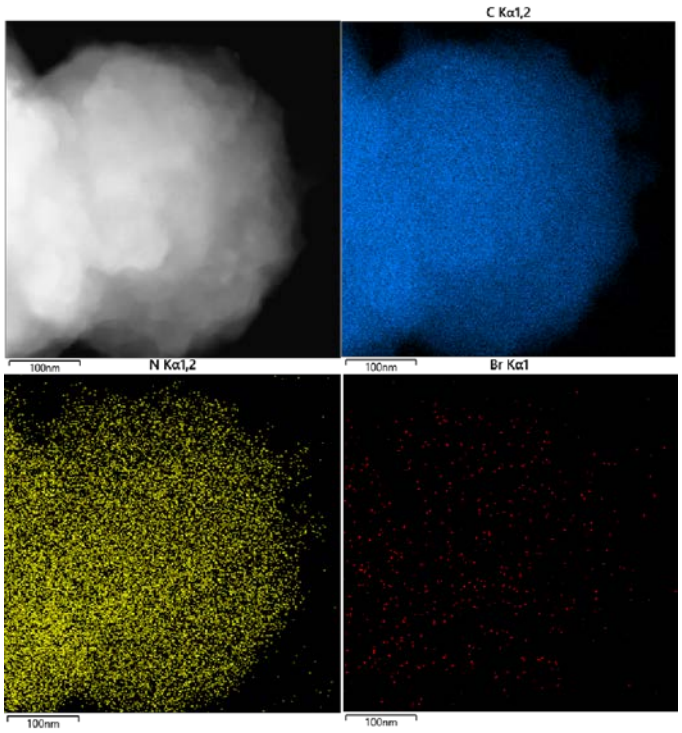

Fig. S19. EDS images of TBE-COF. Blue, yellow and red respectively represent the three elements of C, N, Br.

Section 15. ^{1}H NMR data and spectra for the crude cyclic carbonates

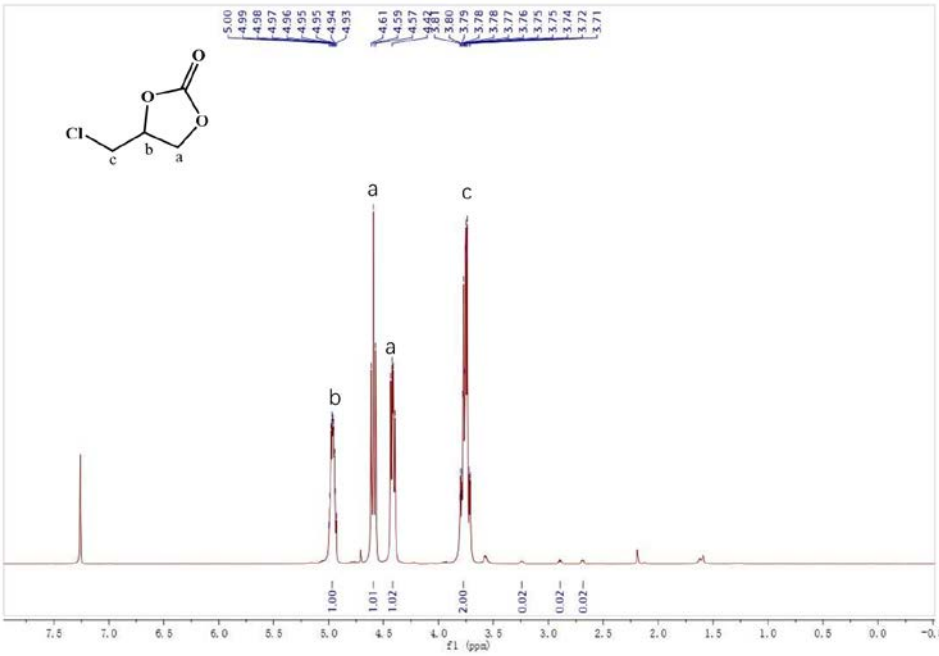

Fig. S20 ^{1}H NMR spectrum of 4-chloromethyl-1,3-dioxolan-2-one NMR (400 MHz, $CDCl_3$): δ 5.09-4.86 (1H, CH), 4.59 (1H, CH_2), 4.42 (1H, CH_2), 3.88-3.58 ppm (2H, CH_2).

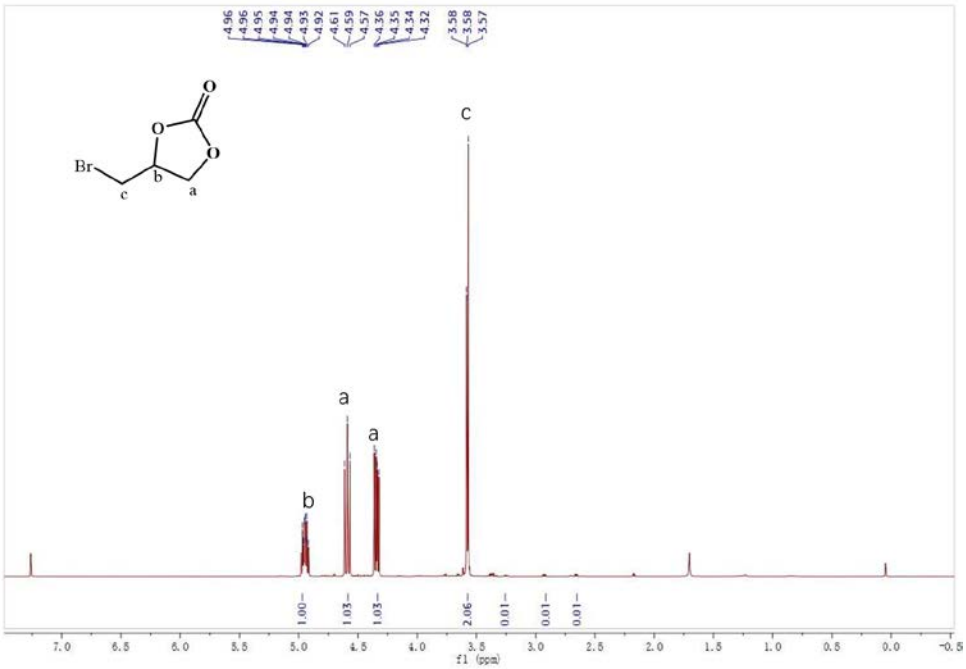

Fig. S21 ^{1}H NMR spectrum of 4-bromomethyl-1,3-dioxolan-2-one (400 MHz, CDCl3): δ 5.09-4.82 (1H, CH), 4.66-4.47 (1H, CH_2), 4.34 (1H, CH_2), 3.64-3.51 ppm (2H, CH_2).

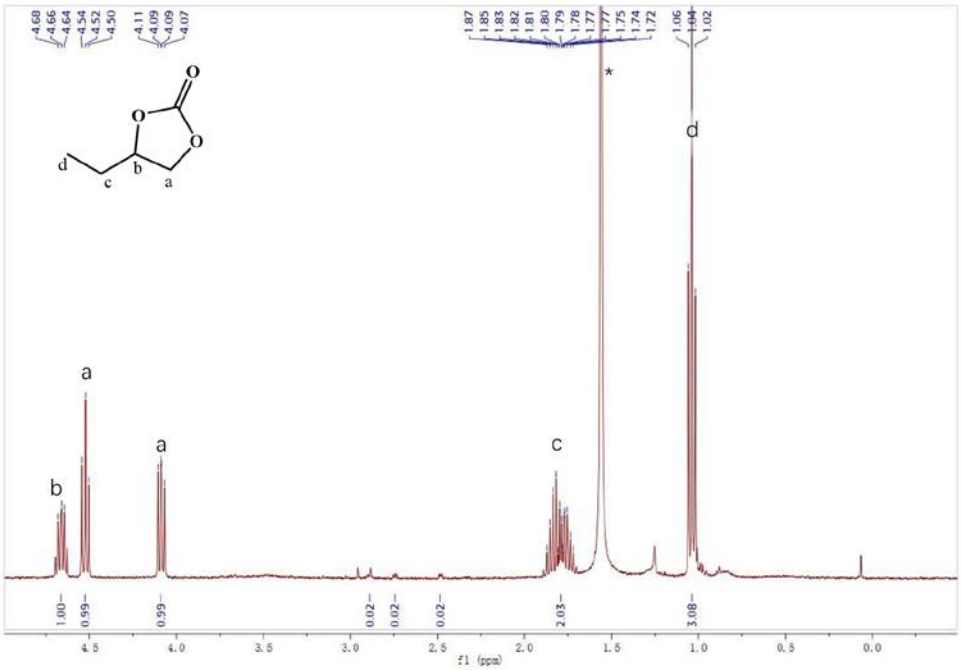

Fig. S22 ^{1}H NMR spectrum of 4-ethyl-1,3-dioxolan-2-one (400 MHz, $CDCl_3$): δ 4.73-4.59 (1H, CH), 4.52 (1H, CH_2), 4.09 (1H, CH_2), 1.89-1.70 (2H, CH_2), 1.07-0.98 ppm (3H, CH_3).

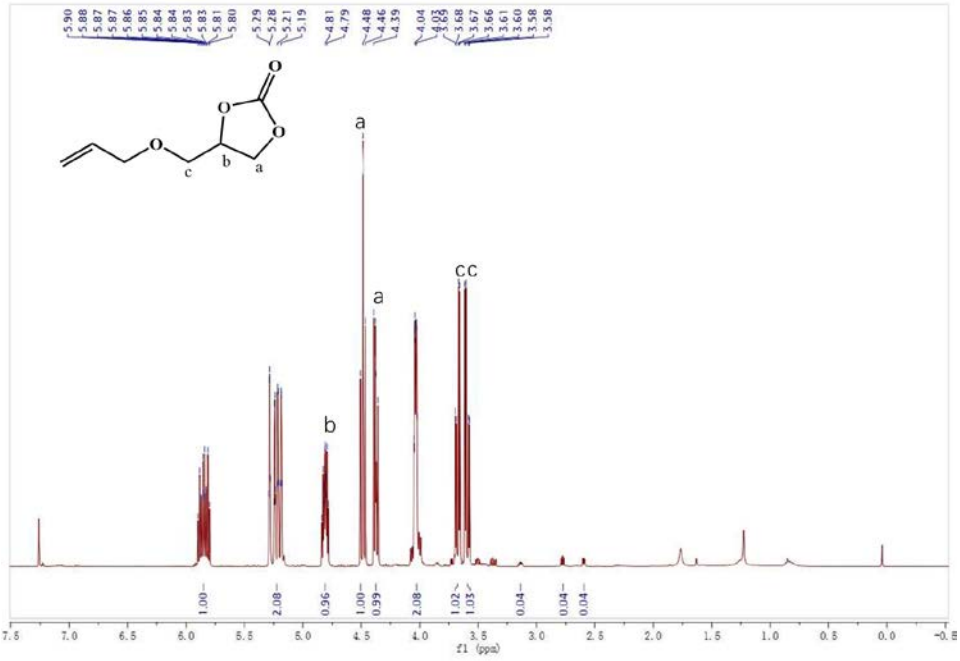

Fig. S23 ^{1}H NMR spectrum of 4-allyloxymethyl-1,3-dioxolan-2-one (400 MHz, $CDCl_3$): δ 5.85 (1H, CH), 5.23 (2H, CH_2), 4.90-4.71 (1H, CH), 4.48 (1H, CH_2), 4.38 (1H, CH_2), 4.03 (2H, CH_2), 3.68 (1H, CH_2), 3.61-3.53 ppm (1H, CH_2).

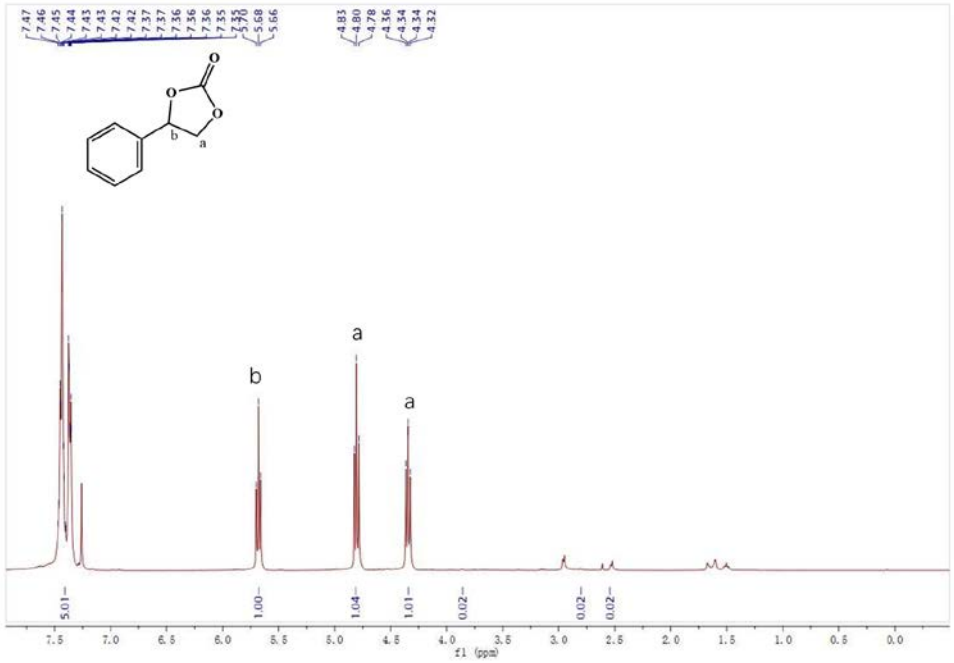

Fig. S24 ^{1}H NMR spectrum of 4-phenyl-1,3-dioxolan-2-one (400 MHz, $CDCl_3$): δ 7.54-7.28 (5H, CH), 5.68 (1H, CH), 4.80 (1H, CH_2), 4.34 ppm (1H CH_2).

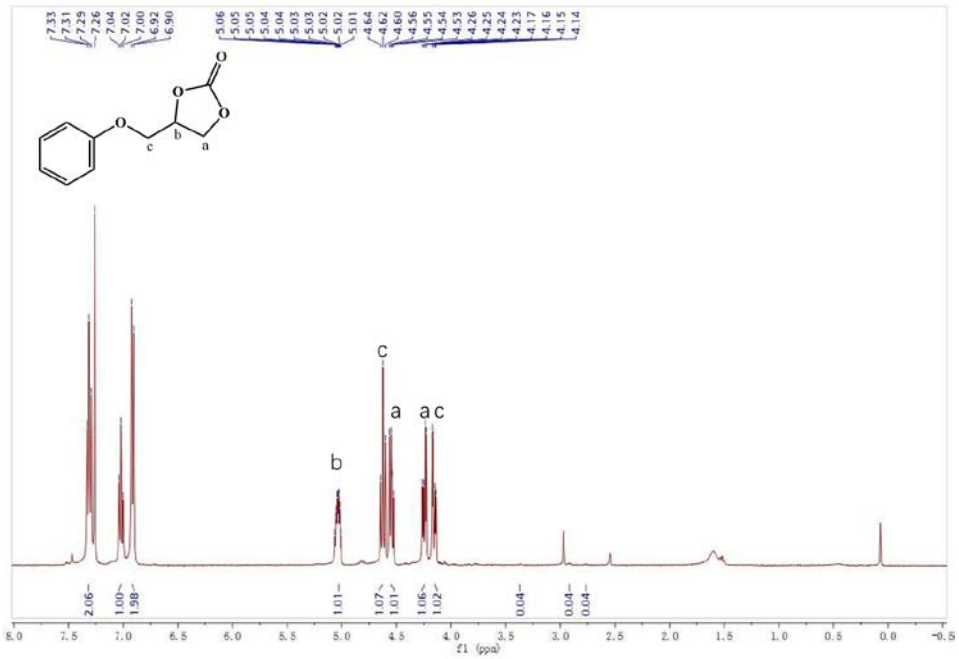

Fig. S25 ^{1}H NMR spectrum of 4-phenoxymethyl-1,3-dioxolan-2-one (400 MHz, $CDCl_3$): δ=7.31 (2H, CH), 7.02 (1H, CH), 6.93-6.89 (2H, CH), 5.07-5.00 (1H, CH), 4.62 (1H, CH_2), 4.54 (1H, CH_2), 4.24 (1H, CH_2), 4.17-4.13 ppm (1H, CH_2).

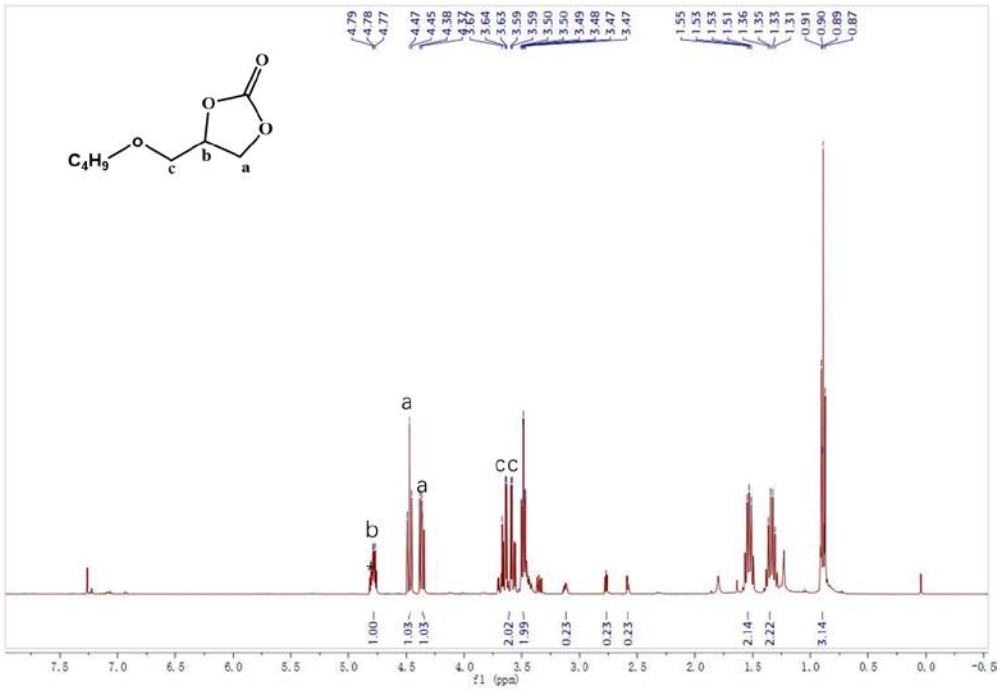

Fig. S26 ^{1}H NMR spectrum of 4-butyloxymethyl-1,3-dioxolane-2-one (400 MHz, $CDCl_3$): δ 4.85-4.73 (1H, CH), 4.47 (1H, CH_2), 4.39-4.29 (1H, CH_2), 3.68-3.56 (2H, CH_2), 3.49 (2H, CH_2), 1.53 (2H, CH_2), 1.34 (2H, CH_2), 0.89 ppm (3H, CH_3).

Section 16. Summary of studies on CO_2 cycloaddition

For this model reaction, we compared the results with other study (Table S9). According to the data listed in Table S9, we could get the conclusion that the TTE-COF could be regarded as a type of potential catalyst for CO_2 chemical fixation. The crystalline structure characteristics of ionic COFs not only provided a high density of ionic active sites but also facilitated their accessibility and then accelerated mass transfer rates during the reaction.

Table S9. Comparison with various catalysts in the performance of the coupling of epichlorohydrin and CO_2.

Entry	Catalyst	Loading	Cocatalyst	Conditions	Yield/%	Ref
1	COF1/$ZnBr_2$	0.1 mol% (Zn)	TBAB	12 h, 80 ℃, 0.1 MPa	99	6
2	Zn/TPA-TCIF(BD)	50 mg	TBAB	10 h, 40 ℃, 0.5 MPa	99	7
3	POM@ImTD-COF	100 mg	TBAB	24 h, 80 ℃, 0.1 MPa	99	8
4	Al-iPOP	0.1 mmol%	------	6 h, 40 ℃, 1.0 MPa	99	9
5	AMIMBr@H2P-DHPhCOF	50 mg	------	24 h, 120 ℃, 1.0 MPa	91	10
6	CTF-0-400-40-1	100 mg	------	4 h, 130 ℃, 0.69 MPa	99	11
7	Pyridyl salicylimine	30 mg	------	24 h, 100 ℃, 0.1 MPa	99	14
8	$Zn_9O_2(OH)_2(pyz)_{12}$	0.5 mol%	TBAB	24 h, 80 ℃, 0.7 MPa	96	15
9	TTE-COF	20 mg	------	20 h, 100 ℃, 0.1 MPa	98	this work

Section 17. Characterizations after catalysis

Table S10. Recycling performance of TTE-COF.

Cycle	Temprature/℃	Residual Weight/mg	Time/h	Yield
1	100	20.0	20	98
2	100	19.9	20	98
3	100	19.8	20	97

4	100	19.8	20	96
5	100	19.6	20	94

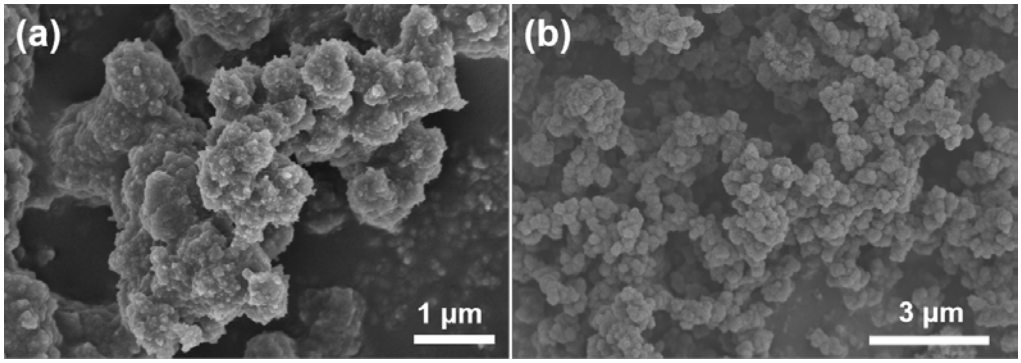

Fig. S27. (a, b) SEM images of TTE-COF after cycloaddition.

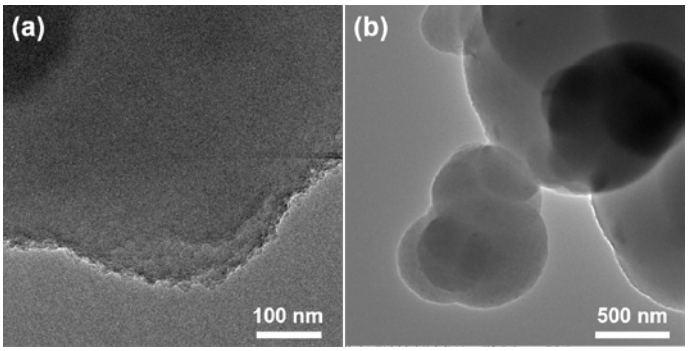

Fig. S28. (a, b) TEM images of TTE-COF after cycloaddition.

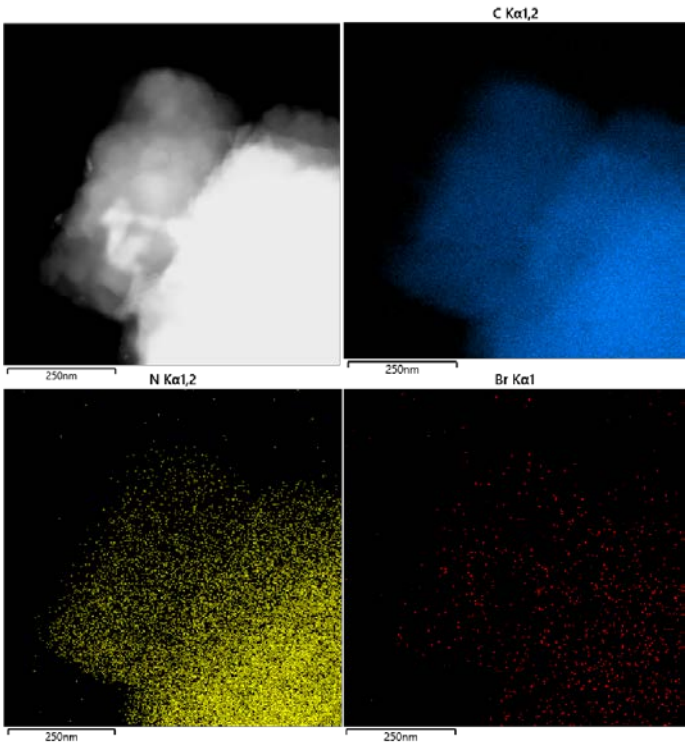

Fig. S29. EDS images after cycloaddition of TTE-COF. Blue, yellow, red respectively represent the elements of C, N, Br.

Section 18. Mechanism for the CO_2 cycloaddition

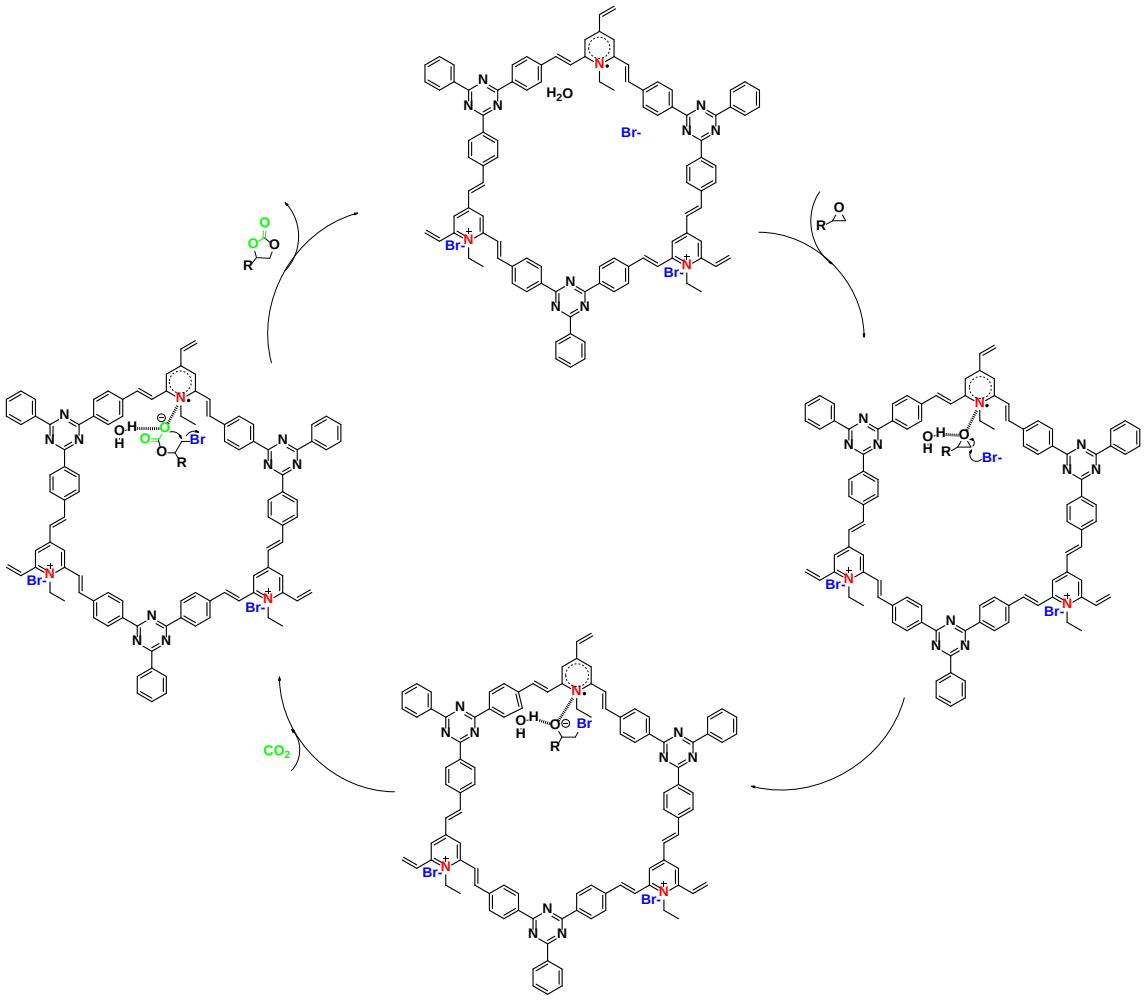

Fig. S30. Possible catalytic mechanism for the CO_2 cycloaddition.

References

1. Meng F C, Bi S, Sun Z B, Jiang B, Wu D Q, Chen J S, Zhang F. Synthesis of ionic vinylene-linked covalent organic frameworks through quaternization-activated knoevenagel condensation. Angewandte Chemie International Edition, 2021, 60: 13614-13620

2. Liu Z Q, Su Q, Ju P Y, Li X D, Li G H, Wu Q L, Yang B. A hydrophilic covalent organic framework for photocatalytic oxidation of benzylamine in water. Chemical

Communications, 2020, 56: 766-769

3. EL-Mahdy A F M, Young C, Kim J, You J, Yamauchi Y, Kuo S W. Hollow microspherical and microtubular [3+3] carbazole-based covalent organic frameworks and their gas and energy storage applications. ACS Applied Materials & Interfaces, 2019, 11: 9343-9354

4. Liu X M, Yang F, Wu L J, Zhou Q, Ren R P, Lv Y K. Ionic liquid-loaded covalent organic frameworks with favorable electrochemical properties as a potential electrode material. Microporous and Mesoporous Materials, 2022, 336: 111906

5. Vyas V S, Haase F, Stegbauer L, Savasci G, Podjaski F, Ochsenfeld C, Lotsch B V. A tunable azine covalent organic framework platform for visible light-induced hydrogen generation. Nature communications, 2015, 6: 8508

6. Dhankhar S S, Nagaraja C M. Porous nitrogen-rich covalent organic framework for capture and conversion of CO_2 at atmospheric pressure conditions. Microporous and Mesoporous Materials, 2020, 308: 110314

7. Puthiaraj P, Kim H S, Yu K, Ahn W S. Triphenylamine-based covalent imine framework for CO_2 capture and catalytic conversion into cyclic carbonates. Microporous and Mesoporous Materials, 2020, 297: 110011

8. Zhang Z R, Yang D H, Qiao S L, Han B H. Synergistic catalysis of ionic liquid-decorated covalent organic frameworks with polyoxometalates for CO_2 cycloaddition reaction under mild conditions. Langmuir, 2021, 37: 10330-10339

9. Chen Y J, Luo R C, Xu Q H, Jiang J, Zhou X T, Ji H B. Charged metalloporphyrin

polymers for cooperative synthesis of cyclic carbonates from CO_2 under ambient conditions. ChemSusChem, 2017, 10: 2534-2541

10. Zhang Y, Hu H, Ju J, Yan Q Q, Arumugam V, Jing X C, Cai H Q, Gao Y N. Ionization of a covalent organic framework for catalyzing the cycloaddition reaction between epoxides and carbon dioxide. Chinese Journal of Catalysis, 2020, 41: 485-493

11. Chen C J, Zhang Y D, Liu K, Liu X Q, Wu L, Zhong H, Dang X J, Tong M M, Long Z Y. In situ construction of phenanthroline-based cationic radical porous hybrid polymers for metal-free heterogeneous catalysis. Journal of Materials Chemistry A, 2021, 9: 7556-7565

12. Liu K, Xu Z X, Huang H, Zhang Y D, Liu Y, Qiu Z H, Tong M M, Long Z Y, Chen G J. In situ synthesis of pyridinium-based ionic porous organic polymers with hydroxide anions and pyridinyl radicals for halogen-free catalytic fixation of atmospheric CO_2. Green Chemistry, 2022, 24: 136-141

13. Katekomol P, Roeser J, Bojdys M, Weber J, Thomas A. Covalent triazine frameworks prepared from 1, 3, 5-tricyanobenzene. Chemistry of Materials, 2013, 25: 1542-1548

14. Subramanian S, Park J, Byun J, Jung Y, Yavuz C T. Highly efficient catalytic cyclic carbonate formation by pyridyl salicylimines. ACS Applied Materials & Interfaces, 2018, 10: 9478-9484

15. Ma F X, Mi F Q, Sun M J, Huang T, Wang Z A, Zhang T, Cao R. A highly stable

Zn_9-pyrazolate metal-organic framework with metallosalen ligands as a carbon dioxide cycloaddition catalyst. Inorganic Chemistry Frontiers, 2022, 9: 1812-1818